Received: 1 February 2026 | Revised: 28 May 2026 | Accepted: 9 July 2026 | Published online: 30 July 2026

RESEARCH ARTICLE

Journal of Optics and Photonics Research
2026, Vol. 00(00) 1–12
DOI: 10.47852/bonviewJOPR62029251

BON VIEW PUBLISHING

First-Principle Calculations of Structural, Electronic, Elastic, and Optical Properties of $XBaCl_3$ (X = In, Tl) Chloro-Perovskites

Shujaat Ali Khan[1], Nasir Rahman[2], Shah Zeb Ullah[1, 3,*], Muhammad Sajjad[1] and Junaid Rehman[1]

[1] *Department of Physics, Kohat University of Science and Technology Kohat, Pakistan*

[2] *Department of Physics, University of Lakki Marwat, Pakistan*

[3] *Department of Physics, Government Post Graduate College Kohat, Pakistan*

Abstract: To investigate the potential of barium-based halide perovskites for optoelectronic applications, we performed first-principles density functional theory calculations on $XBaCl_3$ (X = In, Tl). These calculations were performed using the WIEN2k package, which provides detailed insights into the materials' characteristics. The code provides a silent insight into materials' characteristics and potential improvements. We employed the Full-Potential Linearized Augmented Plane Wave (FP-LAPW) approximation to study the optimized structure, electronic, elastic, and optical properties of $XBaCl_3$ chloro-perovskite compounds. To assess the structural stability, we are applying the Birch–Murnaghan fitting curves, confirming that each compound is structurally stable in its optimal or ground states. The IRelast Package is utilized for evaluating the elastic properties, revealing that the materials are anisotropic, brittle, and mechanically stable. In the analysis of electronic structure, the density of states and band structure were examined. It was discovered that the compounds have an indirect bandgap of 4.9 eV for $InBaCl_3$ and 5.6 eV for $TlBaCl_3$. Examining the total and partial density of states allowed us to trace how individual atomic orbitals shape the overall band structure. Furthermore, we also studied the optical response that comprises the dielectric function, refractive index, absorption coefficient, and reflectivity across an energy range of 0–13.5 eV. The materials are transparent to low-energy photons, absorbing light and exhibiting optical conductivity only in the ultraviolet range. This provides critical insight for developing more efficient and functional high-tech electronics and motivating further experimental investigation.

Keywords: chloro-perovskites, dielectric function, ultraviolet absorption, wide bandgap, WIEN2k

1. Introduction

Materials scientists investigate compounds that are crucial to modern technology, primarily through theoretical research. They intend to advance technologies in sectors such as semiconductors, energy storage, and optics. Despite the vast body of existing scientific knowledge, perovskites continue to offer new and surprising properties [1–4]. Perovskite, a mineral first identified by Gustav Rose in 1839 and named for Lev Perovski, has the basic composition $CaTiO_3$ but follows an ABX_3 structural pattern, with two cations A and B of dissimilar sizes and an anion (X). Perovskites fall into two main categories, oxide (with oxygen as X) and halide (with halogens as X), created by swapping the X-site anion. This substitution at the X-site is the primary source of perovskite diversity, and the distinct traits of oxide versus halide perovskites largely determine their functions and applications [5–7]. Perovskite compounds have elevated noteworthy devotion across diverse scientific and technological domains due to their remarkable and tunable physical properties. Notably, their characteristics such as tunable laser emission [8], ferroelectric behavior [9], phase transition phenomena [10], strong electron–phonon coupling [11], and pronounced crystal field effects [12] are extensively reported. Perovskites also parade an array of cutting-edge functionalities, including high dielectric permittivity [13], piezoelectricity [14], superconductivity [15], and excellent charge transport properties [16]. They also demonstrate intriguing optoelectronic features such as high absorption coefficients [17], extended carrier diffusion spans [18], and imperfection tolerance [19], rendering them effective for solar cells and LEDs. Furthermore, their structural flexibility allows for compositional engineering, enabling the tailoring of electronic band structures and enhancing their applicability in next-generation energy and electronic devices.

Besides the mentioned properties, their ability to act as semiconductors [20], anti-ferromagnetism [21], and usage as scintillating materials have also been reported [22]. Scintillation detectors are widely used for radiation sensing, with ongoing efforts to develop new inorganic scintillators for physics, medical

***Corresponding author:** Shah Zeb Ullah, Department of Physics, Kohat University of Science and Technology Kohat, Pakistan and Department of Physics, Government Post Graduate College Kohat, Pakistan. Email: ph420222002@kust.edu.pk

imaging, and materials science. The operation of a radiation detection device using a single-crystal scintillator is contingent strongly on the physical and scintillation characteristics of the crystal [23, 24]. Scintillators are widely used for their brightness, directivity, and energy sensitivity [25, 26], while chloro-perovskites are gaining interest as promising candidates due to their favorable bandgaps, high absorbance, and low-cost synthesis [27–30]. Alkali-metal doping (Li, Na, K, Rb, Cs) boosts perovskite solar cell performance and efficiency [31, 32]. Furthermore, the incorporation of these metals induces significant modifications in the electronic and thermodynamic properties, resulting in enhanced generation and diffusion of photo-induced charge carriers. This, in turn, contributes to improved long-term stability under ambient conditions [33–37].

The incorporation of alkali metal ions into halide perovskites has been reported to produce structural and optoelectronic adjustments, resulting in superior charge dose, increased luminance, improved humidity resistance, and optimized band orientation in nanocrystalline as well as polycrystalline perovskite thin films [38–40]. Perovskites are studied for solar applications via density functional theory (DFT), a well-established computational tool [41].

In this paper, the fundamental physical properties of ternary $XBaCl_3$ (X = In, Tl) chloro-perovskites have been theoretically studied through the DFT framework. These materials are useful in energy storage, scintillators, and modern devices. To date, no experimental studies on $InBaCl_3$ or $TlBaCl_3$ have been reported, nor have any theoretical investigations using the same method (WIEN2k) been published. However, analogous chloro-perovskites such as $CsCaCl_3$, $CsCaI_3$, and $CsBaCl_3$ have been successfully synthesized, suggesting that $InBaCl_3$ and $TlBaCl_3$ are likely also synthetically feasible [42–44].

The selection of $InBaCl_3$ and $TlBaCl_3$ is motivated by the need for a systematic comparison of how the A-site cation influences the properties of chloro-perovskites. Although both In and Tl belong to Group 13, they differ significantly in ionic radius, electronegativity [45], and relativistic effects [46], enabling a meaningful structure–property correlation. Additionally, while lead-based perovskites raise toxicity concerns [47], In- and Tl-containing chloro-perovskites remain underexplored despite their potential for optoelectronic and radiation detection applications [48, 49]. This study therefore investigates these two compounds to establish their fundamental structural, electronic, and optical characteristics.

2. Computational Method

This study employs first-principles computational analysis. Calculations were performed using the FP-LAPW method within DFT, as implemented in WIEN2K [50]. Structural optimization and elastic properties were obtained using the Perdew-Burke-Ernzerhof Generalized Gradient Approximation (PBE-GGA) functional [51, 52]. Lattice parameters were derived by fitting the energy-volume curve to the Birch–Murnaghan equation (BME) of state [53]. Elastic constants (ECs) were computed using the IRLast package [54]. The TB-mBJ potential was used for exchange-correlation to improve electronic and optical property accuracy. TB-mBJ is an advanced DFT functional that enhances bandgap accuracy [55]. A total of 2000 k-points was employed to sample the first Brillouin zone (BZ) in reciprocal space. The RMT values for each atom were determined with the condition of no overlap. In this study, the muffin-tin radii are 2.72 a.u. (Ba), 2.5 a.u. (X, where X = In or Tl), and 2.4 a.u. (Cl). The self-consistent field calculations met the convergence criterion, with a total energy threshold set to 0.001 mRy. For both compounds, the selected cut-off energy, which divides the valence and core states, is set at −6.0 Ry. Molecular dynamics (MD) calculations were conducted with the Dynamics module in Materials Studio. The compound simulation was run in the microcanonical (NVE) ensemble, starting at 298 K without pressure coupling. Initial atomic velocities were assigned randomly, and the system was propagated with a 1.0 fs integration time step over 15.0 ps (1000 steps). To improve numerical stability, all covalent bonds were constrained using the Fix Bonds setting, and atomic positions were saved only at the final time step. All other force-field choices and simulation settings are provided in the methodology section. To determine the materials' optical characteristics, the study uses the basic complex dielectric function, which is $\mathcal{E}(\omega) = \mathcal{E}_1(\omega) + i\mathcal{E}_2(\omega)$.

3. Results and Discussion

This section presents the results for $XBaCl_3$ (X = In, Tl) chloro-perovskites obtained from the methods described above. Different physical properties of the materials are considered separately.

3.1. Structural properties

We examined the structural properties of the $XBaCl_3$ (X = In, Tl) chloro-perovskites, which have lattice constants of 5.64 Å and 5.88 Å, respectively, and crystallize in the Pm-3m (#221) space group. This study takes advantage of the WIEN2K program. Figure 1 displays the cubic crystal structures of the $XBaCl_3$ (X = In, Tl). Thus, in these compounds, "Ba" is placed at (0.5, 0.5, 0.5), "Cl" atoms are positioned at (0, 0.5, 0.5), and "X = "In" and "Tl" atoms are at coordinates (0, 0, 0). We decided to employ the BME to obtain the most important struc-

Figure 1
The optimized crystal structures of ternary $XBaCl_3$ (X = In, Tl)

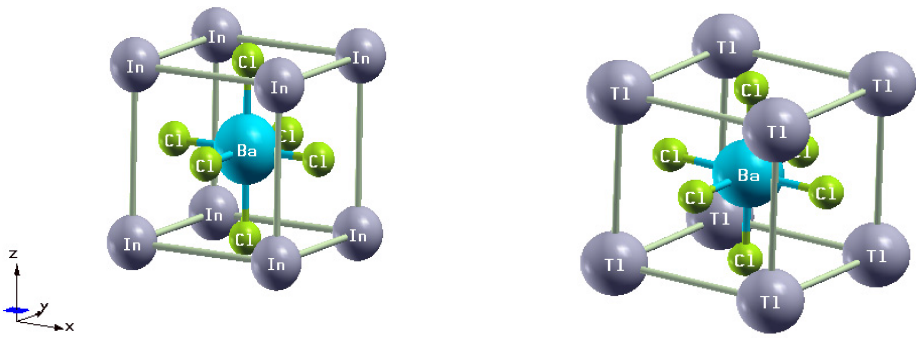

Table 1
The computed optimized lattice constants (a = b = c), bulk modulus (B_o), pressure derivative of bulk modulus (B′), volume at ground state (V_o), and ground state energy (E_o)

Optimized lattice parameters	$InBaCl_3$	$TlBaCl_3$	Zhang et al. [56]	Ullah et al. [57]
Lattice constant (a_o) in A°	5.64	5.98	5.98	5.98
Bulk modulus (B_o) in GPa	17.9641	17.7631	–	17.95
Pressure derivative of bulk modulus (B′) in GPa	4.9418	4.6240	–	5.88
Volume at ground state (V_o) in $(a.u.)^3$	1446.0378	1448.0941	1443.08	1445.63
Ground state energy (E_o) in Ry	–30814.949	–59626.200	–	–59626.2

tural parameters in this work. These parameters comprise the bulk modulus, its pressure derivative, lattice constant, equilibrium unit cell volume, and ground state energy. As seen in the figure, the process is completed by fitting the primitive cell's energy to its volume characteristics.

$$E(V) = \mathrm{Eo} + \frac{B}{B'(B'-1)}\left[V\left(\frac{\mathrm{Vo}}{V}\right)^{B'} - \mathrm{Vo}\right] + \frac{B}{\mathrm{B}'}(\mathrm{V} - \mathrm{Vo}) \quad (1)$$

In Equation (1) B, E_o, V, B', and V_o refer to the optimum values for bulk modulus, total energy, optimal unit cell volume, bulk modulus pressure derivative, and total unit cell volume, respectively. The values of the structural characteristics for the $XBaCl_3$ chloro-perovskite (where X = In or Tl) are given in Table 1 [43]. Figure 2 displays optimization curves obtained from the generalized gradient approximation (GGA) approximation for structural analysis. Table 1 lists the optimal parameters that were discovered when these curves were fitted using the BME. As the unit cell volume increases, the total energy decreases until reaching a minimum at the equilibrium volume, which corresponds to the ground state. The unit cell volume increases when the lattice constant rises.

Table 1 displays the bottom volume state (E_o) corresponding to a specific unit cell volume. It is important to note that the findings of this study cannot be directly compared to any experimental. Substituting In with Tl expands the lattice constant significantly from 5.64 Å to 5.98 Å (~5.6%), reflecting the larger ionic radius of Tl. Mechanically, however, the materials remain remarkably similar, both exhibiting soft compressibility with bulk moduli hovering near 18 GPa. While $TlBaCl_3$ shows a marginal reduction in bulk modulus and pressure derivative (4.94 and 4.62), suggesting slight softening, the overall elastic response is preserved across both compounds. Nonetheless, the accuracy of our findings is supported by the dense sampling of 2000 k-points within the Brillouin zone, a methodology that aligns with established high-precision research.

The MD curves shown in Figure 3 for $InBaCl_3$ (black) and $TlBaCl_3$ (red) show potential energy, non-bonded interaction energy, kinetic energy, and instantaneous temperature fluctuating around approximately constant mean values over 0–15 ps, with no sustained upward/downward drift; such stationary fluctuations are characteristic of dynamically stable systems in which the structure remains intact and the simulation is well behaved [58]. The comparable fluctuation amplitudes in potential and non-bond energies indicate that both compounds maintain similar ionic packing and long-range electrostatic balance under the applied conditions, while the stable kinetic energy and temperature bands suggest consistent thermal equilibration and absence of numerical instability. Overall, the curves support short-timescale dynamical stability for both $InBaCl_3$ and $TlBaCl_3$, with no clear evidence from these diagnostics alone that one is markedly less stable than the other.

In brief, the absence of any significant energy drift or catastrophic failure over the simulation timescale confirms that both the $XBaCl_3$ (X = In, Tl) crystal structures have stable energy and temperature profiles, validating the structural integrity and dynamic robustness of these compounds under the simulated environment.

Figure 2
Optimized curve fitting using the Birch–Murnaghan equation of state for (a) $InBaCl_3$ and (b) $TlBaCl_3$

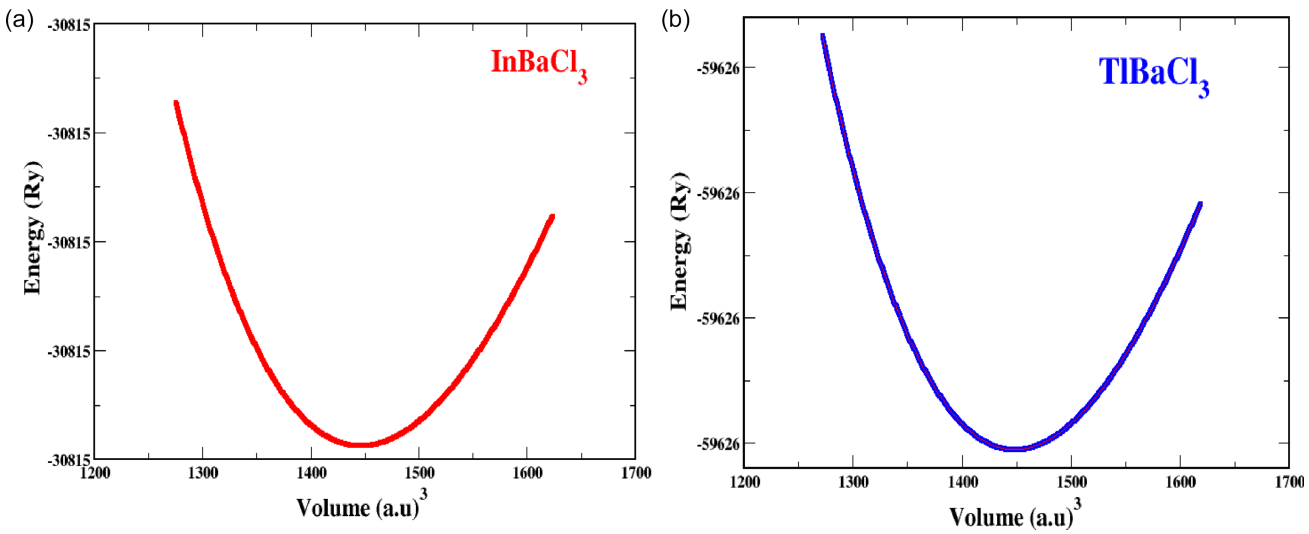

Figure 3
Stability analysis of $XBaCl_3$ (X = In, Tl) using ab initio molecular dynamics

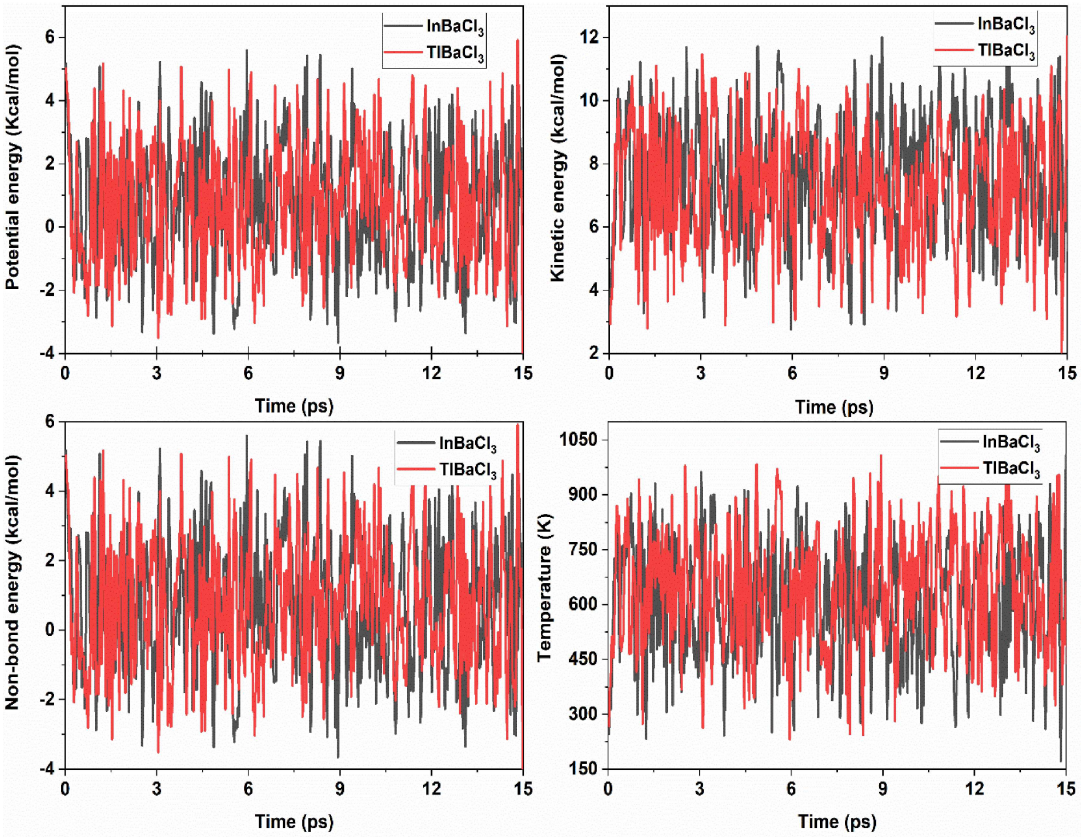

3.2 Electronic properties

The electronic properties of $XBaCl_3$ (X = In, Tl) were explored using band structure and density of states (DOS) calculations. The GGA approximation has been used to compute these characteristics.

1) **Bands structure**

The band structure and DOS determine the electronic properties of chloro-perovskite materials, such as how well they are semiconducting, metallic or insulating, as well as the bonding type and gap energies. The band structure gives valuable evidence about material conductance and acts as a vital connection between electronic and optical capabilities and crystal structure. DFT calculations allow you to establish the band pattern of a material, along the high-symmetry paths in the first BZ using 2000 k-points. The approximation of TB-mBJ predicts that the band structures of the inspected ternary $XBaCl_3$ (X = In, Tl) chloro-perovskite compounds would lie inside the BZ, ranging from −2 eV to +10 eV, as demonstrated by the high-symmetry sites "M-X" depicted in Figure 4. For both compounds, the conduction band minima are positioned at the X symmetry point, while the valence band maxima are at the M symmetry point [59]. $InBaCl_3$ and $TlBaCl_3$ have calculated bandgaps of 4.9 eV and 5.6 eV, showing that they are both indirect bandgap insulators. For $InBaCl_3$, Zhang et al. [56] reported an HSE06 bandgap of 4.178 eV (direct), differing by ~17% from our TB-mBJ value of 4.9 eV (indirect). This discrepancy likely arises from differences in computational code, functionality, and bandgap character. For $TlBaCl_3$, our TB-mBJ bandgap (5.6 eV) agrees within 2% of Ullah et al. [57] (5.51 eV), confirming reproducibility across independent WIEN2k/TB-mBJ calculations. Wide-bandgap semiconductors (e.g., diamond, SiC, $CuAlS_2$ ~3.49 eV, Ga_2O_3 ~4.66 eV) enable higher power, frequency, temperature, and UV operation, with Ga_2O_3 exhibiting the widest tunable spectral range. They are used in transparent electronics, gas sensors, optoelectronics, UV emitters, and as window layers in cascade solar cells to improve UV quantum efficiency [60].

2) **Density of states (DOS)**

In order to deeply comprehend the electronic properties of a solid, analysis of the DOS is essential. This analysis, depicted in Figure 5 for $XBaCl_3$ (X = In, Tl) chloro-perovskites, reports energy from −4 eV to 7 eV. A comparative analysis of the total density of states (TDOS) and partial density of states (PDOS) in Figure 5 reveals that while $InBaCl_3$ and $TlBaCl_3$ share fundamental bonding characteristics, they differ markedly in their deep valence electronic structures. In both compounds, the region immediately surrounding the Fermi level (E_F = 0 eV) in the valence band is enormously dominated by chlorine p-states hybridizing with barium orbitals, forming the primary valence band maximum. Additionally, both materials exhibit a common, sharp resonance in the conduction band at approximately +5.64 eV, driven by unoccupied high-energy states.

However, a critical distinction appears in the lower valence band (−1 to −3 eV). $TlBaCl_3$ displays substantial spectral weight from thallium d-states and f-states that overlap precisely with the secondary Cl-p peaks in this region. This indicates substantial p-d(f) hybridization involving the heavy Tl cation. In contrast, $InBaCl_3$ shows negligible contribution from indium d-states in this energy range, resulting in a spectrum dominated almost exclusively by the

Figure 4
The electronic band structure of $XBaCl_3$ (X = In, Tl) chloro-perovskites

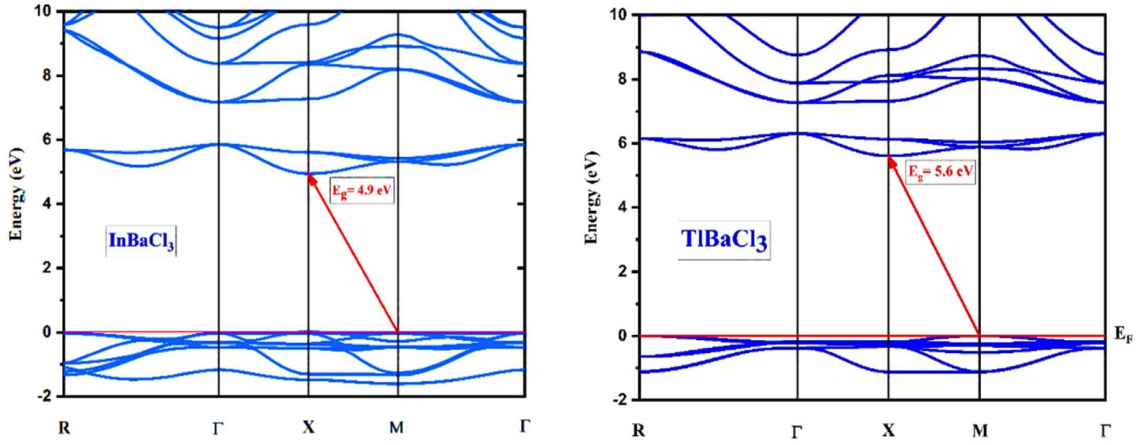

Figure 5
The calculated density of states (DOS) for $InBaCl_3$ and $TlBaCl_3$ chloro-perovskites

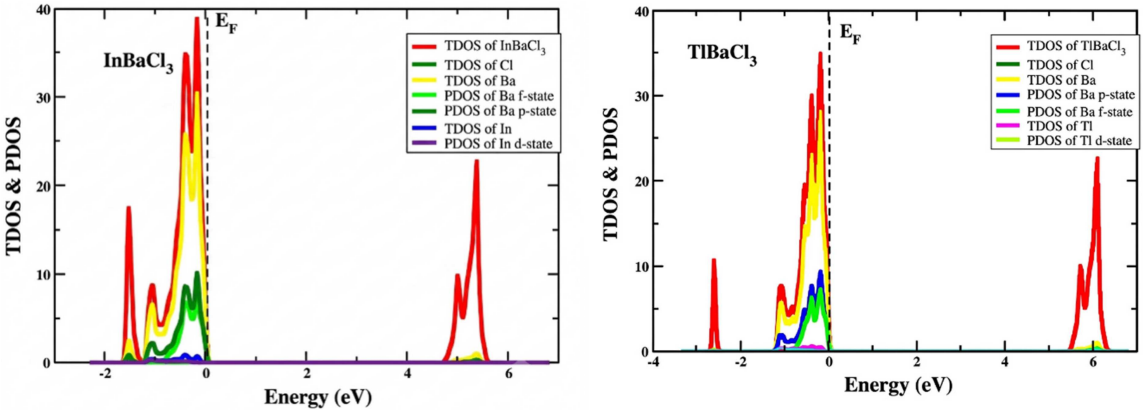

halide and alkaline earth framework without the complex multi-orbital mixing seen in the Tl counterpart.

3.3. Elastic properties

ECs are crucial parameters for understanding a material's mechanical behavior, hardness, and strength, with three independent constants governing the elastic behavior of any cubic crystal. The ECs in this work were found using the IR-Elast program from the Wien2k Package. The calculated EC values for the barium-based perovskite $XBaCl_3$ (X = In, Tl) are shown in Table 2. Based on the Born–Huang criteria, both compounds are mechanically stable, as evidenced by the positive estimated values of the ECs: $(C_{11}-C_{12}) > 0$; $(C_{11} + 2C_{12}) > 0$; $C_{44} > 0$), and the bulk modulus $B = (2C_{12} + C_{11})/3 > 0$ must also fulfill the requirement: $(C_{12} < B < C_{11})$ for mechanical stability, confirming the mechanically stable state of both compounds [61]. Additionally, the C_{11} value is higher than C_{12} and C_{44}, indicating that the compounds are resistant to compression along the x-axis. The hardness of a material is indicated by the bulk modulus (B). A higher B value corresponds to greater hardness. The higher bulk modulus of $InBaCl_3$ shows that it is harder than $TlBaCl_3$. Consequently, when the compounds undergo compression, $InBaCl_3$ withstands greater volume change from all directions than $TlBaCl_3$. $InBaCl_3$ can withstand greater transverse deformation than $TlBaCl_3$ because of its high shear modulus (G) [62]. In order to ascertain "B" and "G" generally, the estimations of Voigt and Reuss are frequently employed [63]. One may assess a material's ductility and brittleness using Pugh's ratio (B/G). The material will be ductile if the B/G is farther than 1.75; otherwise, it will be brittle [64]. The Pugh's ratio computation results are shown in Table 2. The brittleness of the materials under investigation is shown by the calculated Pugh's ratio values. The anisotropy factor (A) provides an explanation for the material's anisotropic nature [65]. The estimated value of "A" differs from "1," indicating that both compounds are anisotropic [66, 67]. The Cauchy pressure parameter $(C_{12}-C_{44})$ determines a material's bonding behavior; a positive value specifies ionic bonding, whereas a negative value directs covalent bonding. The negative results of the Cauchy pressure for $InBaCl_3$ indicate the covalent nature of bonding, while the positive value of the Cauchy pressure for $TlBaCl_3$ indicates the ionic nature of bonding [68]. Formulas for the anisotropy factor, Young's and Reuss approximations, Poisson's ratio, compressibility, and shear moduli are listed below:

$$G = \frac{1}{2}(G_V + G_R) \tag{2}$$

$$G_V = \frac{1}{5}(C_{11} - C_{12} + 3C_{44}) \tag{3}$$

$$G_R = \frac{5C_{44}(C_{11} - C_{12})}{4C_{44} + 3(C_{11} - C_{12})} \tag{4}$$

$$E = \frac{9GB}{3B + G} \tag{5}$$

$$v = \frac{3B - 2G}{2(3B + G)} \tag{6}$$

$$A = \frac{2C_{44}}{(C_{11} - C_{12})} \tag{7}$$

$$B = \frac{(2C_{12} + C_{11})}{3} \tag{8}$$

Shear modulus, Vogt's G_v and Reuss G_R, Young's modulus Y, Poisson's ratio *v*, anisotropy factor A, and bulk modulus B are in Equations (2)–(8), respectively.

In comparing the mechanical properties of $InBaCl_3$ and $TlBaCl_3$ in Table 2, significant differences emerge regarding their elasticity and structural stability. $InBaCl_3$ exhibits much higher longitudinal stiffness, with a C_{11} of 84.15 GPa compared to 43.91 GPa for $TlBaCl_3$. The exceptional feature of $InBaCl_3$ is its negative C_{12} (−14.47 GPa) and negative Poisson's ratio (−0.102), identifying it as an auxetic material [69, 70], whereas $TlBaCl_3$ behaves traditionally with a positive ratio of 0.364. While both materials share nearly identical bulk moduli (B ~18 GPa), $InBaCl_3$ is significantly more rigid in terms of shear (G) and Young's modulus (E), being roughly six and four times stiffer than $TlBaCl_3$, respectively. Furthermore, the B/G ratio classifies $InBaCl_3$ as a brittle material (0.497), while $TlBaCl_3$ is highly ductile (3.33).

Zhang et al. [56]'s results align nearly perfectly with $TlBaCl_3$, describing a soft, ductile material, while Ullah et al. [57] report a much stiffer, stronger compound with a different elastic preference. $InBaCl_3$ stands apart as a rigid auxetic material. Overall, the three studies reveal distinct mechanical profiles ranging from ductile to stiff and auxetic behavior.

3.4. Optical properties

The optical properties of $XBaCl_3$ (X = In, Tl) chloro-perovskites are extensively discussed in this section, focusing on various parameters. It has been established that both $InBaCl_3$ and $TlBaCl_3$ compounds are insulators with an indirect bandgap, determined through their electronic properties and band structure. Consequently, these materials are well-suited for photosensitive applications. The following equations were used to calculate the optical properties using the dielectric constant [71, 72].

$$\varepsilon(\omega) = \varepsilon_1(\omega) + i\varepsilon_2(\omega) \tag{9}$$

$$n(\omega) = \left[\frac{\varepsilon_1(\omega)}{2} + \frac{\sqrt{\varepsilon_1{}^2(\omega) + \varepsilon_2{}^2(\omega)}}{2}\right]^{\frac{1}{2}} \tag{10}$$

$$k(\omega) = \left[\frac{-\varepsilon_1(\omega)}{2} + \frac{\sqrt{\varepsilon_1{}^2(\omega) + \varepsilon_2{}^2(\omega)}}{2}\right]^{\frac{1}{2}} \tag{11}$$

$$I(\omega) = \frac{2\omega}{c} k(\omega) \tag{12}$$

$$R(\omega) = \frac{(1-n)^2 + k^2}{(1+n)^2 + k^2} \tag{13}$$

$$\sigma(\omega) = \frac{\hbar\omega\varepsilon_0\varepsilon_2(E)}{\hbar} \tag{14}$$

1) **Dielectric function**

Analyzing the dielectric function reveals key optical properties of $InBaCl_3$ and $TlBaCl_3$. This complex function, including real and imaginary parts, depicts how materials retort to electromagnetic fields and how light propagates through them. Both materials show consistent spectral patterns in their real dielectric functions, and the function is essential for assessing optical performance across all energies [73, 74]. In Figure 6, the "$\varepsilon_1(\omega)$" curves extend from 0 eV to 13 eV of incoming photon energy, exhibiting an aggregate positive peak of 4.9 for $InBaCl_3$ and 5.6 for $TlBaCl_3$ at low photon energy limits. Between 8 eV and 13 eV input photon energy, both $XBaCl_3$ (X = In, Tl) reach negative highest values of approximately −1 for $InBaCl_3$ and −2 for $TlBaCl_3$, suggesting total reflection within these energy ranges. $InBaCl_3$ has a real static "(0)" dielectric function of 2.3, while $TlBaCl_3$ has a

Table 2
The investigated mechanical parameters for $XBaCl_3$ (X = In, Tl) ternary chloro-perovskites

Mechanical properties	$InBaCl_3$	$TlBaCl_3$	Zhang et al. [56]	Ullah et al. [57]
C_{11} (GPa)	84.15	43.91	42.61	115.41
C_{12} (GPa)	–14.47	5.21	4.71	63.22
C_{44} (GPa)	30.83	1.43	1.91	47.29
B (GPa)	18.40	18.11	17.78	21.32
v	–0.102	0.364	0.35	0.30
C_{12}–C_{44} (GPa)	–45.29	3.78	2.8	16.18
G (GPa)	36.99	5.43	5.86	37.26
E (GPa)	66.45	14.80	15.80	96.89
A	0.618	0.074	0.10	1.81
B/G	0.497	3.33	2.96	2.16

value of 2. The imaginary component $\varepsilon_2(\omega)$ is crucial for evaluating optical conversions from the VB to the CB [75]. Figure 6 depicts the "$\varepsilon_2(\omega)$" spectrum for the examined substances. The maximum peaks of $InBaCl_3$ and $TlBaCl_2$ in the 0 to 13 eV photon energy range are 4 and 6.8, respectively. The "$\varepsilon_2(\omega)$" begins at zero at 4.9 eV for $InBaCl_3$ and 5.6 eV for $TlBaCl_3$, indicating the absorption threshold. It achieves its extreme magnitude of 4 at 5 eV for $InBaCl_3$ and 6.8 at 8.7 eV for $TlBaCl_3$; consequently, this implies that the ultraviolet (UV) range is where absorption is supreme. Due to their UV absorption, these materials have intriguing applications in optoelectronics, such as scintillators.

2) **Optical conductivity**

Optical conductivity relates the applied electric field amplitude to the induced current density at a given frequency [76]. Figure 6 shows the optical conductivity spectra calculated for both chloro-perovskite compounds $XBaCl_3$ (X = In, Tl) over a spectrum of incoming photons from 0 eV to 13.5 eV. Figure 6 clearly shows that optical conductivity begins at incoming photon matching the electronic bandgap. The maximal optical conductivity of $InBaCl_3$ is 3300 $\Omega^{-1}cm^{-1}$ at a photon energy of 6.8 eV, whereas $TlBaCl_3$ is 8000 $\Omega^{-1}cm^{-1}$ at an input photon intensity of 8.5 eV. Both $InBaCl_3$ and $TlBaCl_3$ have strong optical conductivity at high energy levels, indicating that they might be used in UV-based optical systems.

3) **Absorption coefficient**

Figure 6 shows the computed absorption coefficient, representing light absorbed per unit length [77]. The absorption coefficient spectrum produced by the TB-mBJ method is shown in this diagram. It illustrates the behavior of I(ω) (absorption coefficient) and its resemblance to the dielectric strength $\varepsilon(\omega)$. It is discovered that there was no light absorption beyond the threshold energy, as predicted, since electronic band transitions from the VB to the CB cannot be produced beneath the bands. The critical ranges of I(ω) for both $InBaCl_3$ and $TlBaCl_3$ chloro-perovskites exceed the bandgap values determined from the band structure calculations. At incoming photons of 12 eV and 8.8 eV, the maximal peak values of absorption for $InBaCl_3$ and $TlBaCl_3$ are at 115×10^4/cm and 172×10^4/cm, respectively, which renders them a better choice for scintillators in the UV range and for lenses at low frequencies [78].

4) **The refractive index**

The refractive index n(ω), derived from the dielectric function, quantifies light bending and improves understanding of

Figure 6
The calculated optical properties for $XBaCl_3$ (X = In, Tl) chloro-perovskites

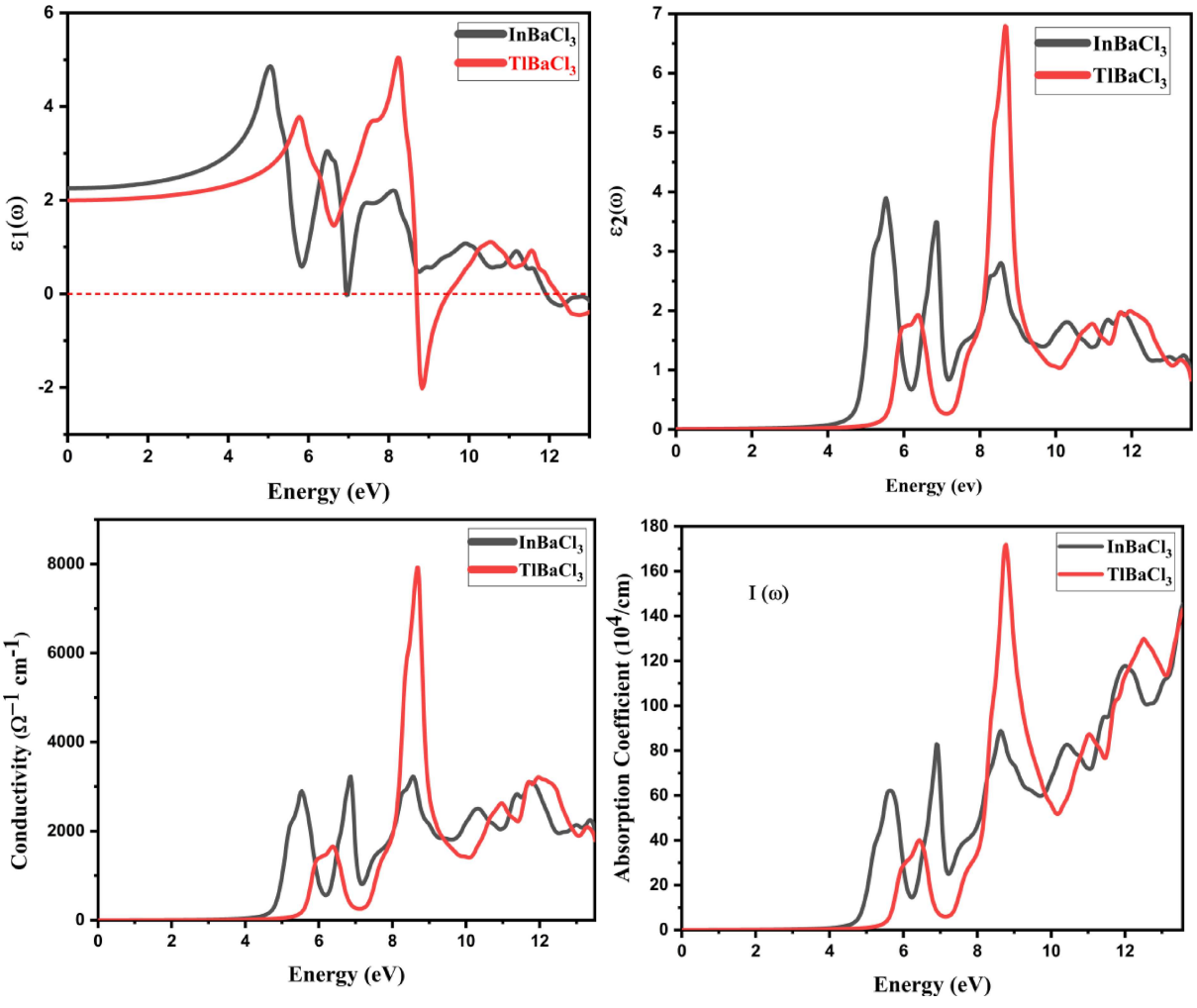

Figure 6
(*Continued*)

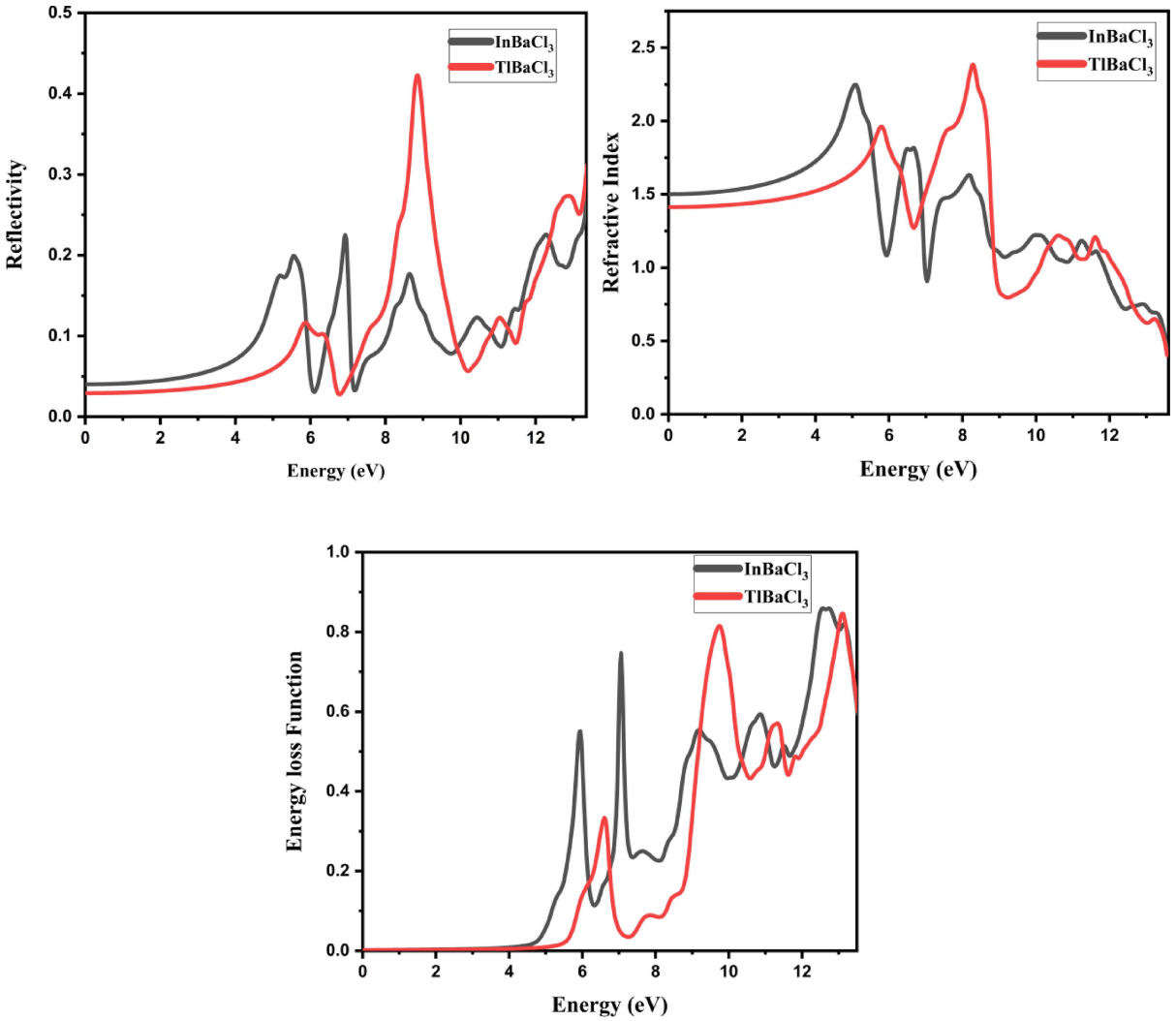

light-material interactions [79]. Figure 6 displays the refractive indices for $XBaCl_3$ (X = In, Tl) chloro-perovskites. The static refractive index n(0) is 1.5 for $InBaCl_3$ and 1.4 for $TlBaCl_3$. The maximum values of 2.26 for $InBaCl_3$ and 2.38 for $TlBaCl_3$ were achieved above the zero frequency. The refractive index exceeds one due to photon deceleration from electron interactions. A material's refractive index determines the delay in photon travel time through the material. This shows that both compounds are good optical refractors.

5) **Optical reflectivity**

Reflectivity is a measure of a material's ability to reflect incident energy from its surface [80]. According to Equation (13), the spectrum curves for R(ω) (reflectivity) of $XBaCl_3$ (X = In, Tl) chloro-perovskites are depicted in Figure 6. The static standards of R (0) for $InBaCl_3$ and $TlBaCl_3$ compounds are 0.04 and 0.03 at 6.8 eV and 8.7 eV, respectively. As photon energy increases, photons are more likely to be reflected from the material's surface. As photon energy increases, both $InBaCl_3$ and $TlBaCl_3$ exhibit increased optical reflectivity, as seen in Figure 6. In the 0–5 eV photon energy range, optical reflectivity is modest, and as photon energy rises, the R(w) spectra for the two substances climb, achieving maximum values of 0.45 for $InBaCl_3$ and 0.48 for $TlBaCl_3$ in the high-photon-energy UV range (13.5 eV), showing that both compounds have relatively low reflectivity at low photon frequencies.

6) **The energy loss function**

The energy loss function (ELF) measures electron energy lost through collisions with other electrons or the lattice [81]. It is computed using the imaginary component of the inverted dielectric functions and provides useful information related to a material's plasmonic, intra-band, and inter-band characteristics. The ELF for $InBaCl_3$ and $TlBaCl_3$ is presented in Figure 6, demonstrating the different energy loss properties of the materials. The ELF remains zero from 0 eV up to the bandgap energy (4.9 eV for $InBaCl_3$ and 5.6 eV for $TlBaCl_3$), indicating no energy loss below the absorption edge. Above these thresholds, the ELF increases, peaking at 12.6 eV for $InBaCl_3$ and 13 eV for $TlBaCl_3$. ELF indicates material response to fields and reveals plasmonic features.

4. Conclusion

DFT, as implemented in WIEN2k, was employed to determine the materials' structural, elastic, electronic, and optical properties. By fitting the BME of the state, it has been ascertained

that $InBaCl_3$ and $TlBaCl_3$ exhibit stable cubic structures. The computed optimized lattice constants for $XBaCl_3$ (X = In, Tl) are 5.64 Å and 5.98 Å, respectively, demonstrating the structural stability at the optimized lattice constants. The ground state energy and lattice characteristics, including bulk moduli and derivatives of bulk moduli, decrease when the metallic cation changes from In to Tl. The computed anisotropy factor "A" confirms that $XBaCl_3$ exhibits significant elastic anisotropy. While the Born criteria verify their mechanical stability, the calculated B/G ratios (Pugh's criterion) classify that $InBaCl_3$ is brittle while $TlBaCl_3$ is ductile in nature. The results of these compounds' band structure calculations show wide indirect energy bandgaps, resulting in insulating properties: 4.9 eV ($M - X$) for $InBaCl_3$ and 5.6 eV ($M - X$) for $TlBaCl_3$. The role of various elemental states in the band structure was determined using PDOS and TDOS. The insulating properties of these compounds facilitate the investigation of their optical properties, which include strong reflectivity at high energies, high absorption coefficients, and high refractive indices. The analysis of their optical characteristics in the energy range of 0 eV to 13.5 eV indicates that both compounds are transparent to visible photons and optically active in the UV region, suggesting applications such as anti-reflection coatings, lenses, and scintillators. This combination of properties is not a drawback but rather a fingerprint for specialized applications. Specifically, the sharp UV absorption edges and high absorption coefficients (up to 1.7×10^6 cm^{-1}) for $InBaCl_3$ and $TlBaCl_3$ as strong candidates for solar-blind UV photodetectors and high-performance scintillation detectors, where wide bandgaps reduce thermal noise. The low visible-range refractive index (n_o = 1.4–1.5) and low reflectivity (R_o = 0.03 to 0.04) suggest utility as anti-reflective coatings, while the high deep-UV reflectivity ($R > 0.45$) supports applications in UV optics and lithography mirrors. Furthermore, the low static dielectric constant (ε_1 (0) = 2.0 to 2.3) and mechanical stability (satisfying Born–Huang criteria) make them potentially useful as interlayer dielectric materials in microelectronics. This comprehensive and systematic calculation of $XBaCl_3$ (X = In, Tl) offers worthwhile insights into the potential of "Ba"-based chloro-perovskites, motivating experimental synthesis and device prototyping for these UV-centric optoelectronic applications.

Ethical Statement

This study does not contain any studies with human or animal subjects performed by any of the authors.

Conflicts of Interest

The authors declare that they have no conflicts of interest to this work.

Data Availability Statement

Data sharing is not applicable to this article as no new data were created or analyzed in this study.

Author Contribution Statement

Shujaat Ali Khan: Conceptualization, Methodology, Software, Validation, Investigation, Writing – original draft, Writing – review & editing, Visualization. **Nasir Rahman:** Software, Validation, Resources, Writing – original draft, Writing – review & editing, Supervision. **Shah Zeb Ullah:** Conceptualization, Writing – original draft, Writing – review & editing, Visualization. **Muhammad Sajjad:** Validation, Resources, Supervision, Project administration. **Junaid Rehman:** Validation, Formal analysis, Writing – review & editing, Visualization.

References

[1] Husain, M., Ullah, A., Algahtani, A., Tirth, V., Al-Mughanam, T., Alghtani, A. H., . . . , & Rahman, N. (2023). Insight into the structural, mechanical and optoelectronic properties of ternary cubic barium-based $BaMCl_3$ (M = Ag, Cu) chloroperovskites compounds. *Crystals*, *13*(1), 140. https://doi.org/10.3390/cryst13010140

[2] Grandhi, G. K., Jagadamma, Krishnan., Sugathan, L., V, Al-Anesi., Manna, B., D, & Vivo, P. (2023). Lead-free perovskite-inspired semiconductors for indoor light-harvesting – The present and the future. *Chemical Communications*, *59*(56), 8616–8625. https://doi.org/10.1039/D3CC01881D

[3] Juhi, J., Saski, M., Kochaniec, M. K., Wieczorek, W., Dominko, R., & Lewiński, J. (2025). Exploring metal halide perovskites as active architectures in energy storage systems. *Journal of Materials Chemistry A*, *13*(45), 38753–38789. https://doi.org/10.1039/D5TA04267D

[4] Usman, T., Khan, S., Khan, M. Y., Iqbal, J., Li, X., Khan, S. A., & Shah, A. H. (2026). Insights into $RbSrX_3$ (X = Cl, Br, I) halide perovskites: First-principles study on their potential for optoelectronic and thermoelectric applications. *Canadian Journal of Chemistry*, *104*(3), 276–288. https://doi.org/10.1139/cjc-2025-0123

[5] Li, X., Hu, E., Wang, F., Lund, P., Zhu, B., & Wang, J. (2024). Proton conductor NASICON-structure Li_{1+x} $Cd_{x/2}$ $Zr_{2-x/2}$ $(PO_4)_3$ as solid electrolyte for intermediate-temperature fuel cells. *Journal of Materials Chemistry A*, *12*(8), 4796–4805. https://doi.org/10.1039/d3ta05182j

[6] Shah, I., Junaid, A., Fawad, U., Rehman, D., Khan, Z., Khan, S. A., & Ullah, S. Z. (2025). Structural, mechanical, anisotropy, electronic and optical insights into $BaCuX_3$ (X = Br, I) perovskites for next-generation photovoltaics. *Journal of Inorganic and Organometallic Polymers and Materials*, *35*(10), 8160–8174. https://doi.org/10.1007/s10904-025-03791-8

[7] Matheu, R., Vigil, J. A., Crace, E. J., & Karunadasa, H. I. (2022). The halogen chemistry of halide perovskites. *Trends in Chemistry*, *4*(3), 206–219. https://doi.org/10.1016/j.trechm.2021.12.002

[8] Shi, Y., Deng, X., Gan, Y., Xu, L., Zhang, Q., & Xiong, Q. (2025). Ten years of perovskite lasers. *Advanced Materials*, *37*(25), 2413559. https://doi.org/10.1002/adma.202413559

[9] Liu, J., Du, F., Wu, L., & Fang, X. (2026). Ferroelectric-configured in-sensor dynamic computing with 2D perovskites for dim object recognition. *Advanced Materials*, *38*(10), e20823. https://doi.org/10.1002/adma.202520823

[10] Yang, M., Ge, W., Guo, Y., Li, J., & Li, Y. (2025). Phase transition behavior enabling reversible luminescence in the novel Sb^{3+} doped double perovskite Cs_2KInCl_6 for advanced anti-counterfeiting applications. *Journal of Alloys and Compounds*, 181218. *1032* https://doi.org/10.1016/j.jallcom.2025.181218

[11] Nonato, A., Rodríguez-Hernández, J. S., Abreu, D. S., Soares, C. C. S., Gómez, M. A. P., García-Fernández, A., . . . , & Paschoal, C. W. A. (2025). Strong electron–phonon coupling and lattice dynamics in one-dimensional $[(CH_3)_2NH_2]PbI_3$ hybrid perovskite. *Chemistry of Materials*, *37*(3), 1013–1026. https://doi.org/10.1021/acs.chemmater.4c02670

[12] Wang, S., Lian, H., Yang, Y., Wu, Z., Li, Y., Ling, H., . . . , & Xu, T. (2025). Morphological engineering for

high-performance perovskite field-effect transistors. *FlexMat*, *2*(1), 82–106. https://doi.org/10.1002/flm2.39

[13] Chouhan, H., Chouhan, M., Prasad, S., Parida, R., & Parida, B. N. (2026). Structural, dielectric, and ferroelectric properties of perovskite-based composite materials: A review. *Synthetic Metals*, *319*, 118163. https://doi.org/ 10.1016/j.synthmet.2026.118163

[14] Ong, A. J., Li, Y., Das, S., Lighthouse, M., Tok, A. I. Y., Lee, P. S., . . . , & Etgar, L. (2026). Lead-free Ruddlesden–Popper double perovskites for high-performance and stable piezoelectric sensors. *ACS Applied Electronic Materials*, *8*(7), 2996–3006. https://doi.org/10.1021/acsaelm.5c02727

[15] Isha, ., Singh, D., Singh Kunwar, H., Karmakar, S., Sarker, D., Sonvane, Y., . . . , & Kumar Yogi, A. (2026). Enhanced electron–phonon coupling due to layered-perovskites octahedral tilting in hole doped cuprate superconductor. *Journal of Physics: Condensed Matter*, *38*(14), 145402. https://doi.org/10.1088/1361-648X/ae574f

[16] Yasir, M. A., Shahzadi, S., Saeed, U., Gassoumi, A., Noor, N. A., Mumtaz, S., & Laref, A. (2026). A first-principles insight to explore the optoelectronic, thermodynamic, and transport properties of ferromagnetic double perovskites Li_2CuOsX_6 (X = Cl, Br) for energy conversion applications. *Journal of Inorganic and Organometallic Polymers and Materials*, *36*(1), 279–298. https://doi.org/10.1007/s10904-025-03937-8

[17] Kim, J., Jung, E. D., You, J., Lee, J., Park, B. C., Snaith, H. J., . . . , & Lee, B. R. (2025). Perovskites for next-generation colour conversion displays. *Nature Electronics*, *8*(10), 886–894. https://doi.org/10.1038/s41928-025-01456-5

[18] Li, S., Yang, X., Cheng, S., Yang, Y., Li, H., Zheng, Z., . . . , & Wang, Z. (2025). Solvent engineering enables tin-lead perovskite films with long carrier diffusion lengths and reduced tin segregation. *Nature Communications*, *16*(1), 8072. https://doi.org/10.1038/s41467-025-63532-w

[19] Liu, G., Ghasemi, M., Wei, Q., Jia, B., Yang, Y., & Wen, X. (2025). Dynamic defect tolerance in metal halide perovskites: From phenomena to mechanism. *Advanced Energy Materials*, *15*(18), 2405239. https://doi.org/10.1002/aenm.202405239

[20] Gong, Y.-P., Chen, X.-X., Huang, G.-Z., Zhang, W.-X., & Chen, X.-M. (2022). Ferroelasticity, thermochromism, semi-conductivity, and ferromagnetism in a new layered perovskite: $(4\text{-fluorophenethylaminium})_2[CuCl_4]$. *Journal of Materials Chemistry C*, *10*(14), 5482–5488. https://doi.org/10.1039/D2TC00335J

[21] Mehmood, S., & Ali, Z. (2022). New anti-ferromagnetic tri-transition quaternary perovskites for magnetic cloaking and spintronic applications. *Materials Chemistry and Physics*, *282*, 125915. https://doi.org/10.1016/j.matchemphys.2022.125915

[22] Moseley, O. D. I., Doherty, T. A. S., Parmee, R., Anaya, M., & Stranks, S. D. (2021). Halide perovskites scintillators: Unique promise and current limitations. *Journal of Materials Chemistry C*, *9*(35), 11588–11604. https://doi.org/10.1039/D1TC01595H

[23] Hua, R., Lei, B., Xie, D., & Shi, C. (2003). Synthesis of the complex fluoride $LiBaF_3$ and optical spectroscopy properties of $LiBaF_3$:M(M = Eu, Ce) through a solvothermal process. *Journal of Solid State Chemistry*, *175*(2), 284–288. https://doi.org/10.1016/S0022-4596(03)00282-2

[24] Wen, X., Wang, Q., Li, W., Li, Y., Cheng, S., Wang, J., . . . , & Wu, Y. (2023). Synthesis and characterization of all-inorganic perovskite CsEuBr3 single-crystal scintillator. *Physica Status Solidi (RRL)–Rapid Research Letters*, *17*(3), 2200341. https://doi.org/10.1002/pssr.202200341

[25] Bouhmaidi, S., Pingak, R. K., Azouaoui, A., Harbi, A., Moutaabbid, M., & Setti, L. (2023). Ab initio study of structural, elastic, electronic, optical and thermoelectric properties of cubic Ge-based fluoroperovskites $AGeF_3$ (A = K, Rb and Fr). *Solid State Communications*, *369*, 115206. https://doi.org/10.1016/j.ssc.2023.115206

[26] Song, X., Li, K., Liu, D., & Guan, J. (2025). Exceptional thermoelectric performance and strong high-order phonon anharmonicity in the ternary tellurides X AgTe (X = K, Rb, Cs). *Physical Review B*, *111*(19), 195209. https://doi.org/10.1103/PhysRevB.111.195209

[27] Murshed, M. N., El Sayed, M. E., Naji, S., & Samir, A. (2021). Electronic and optical properties and upper light yield estimation of new scintillating material $TlMgCl_3$: Ab initio study. *Results in Physics*, *29*, 104695. https://doi.org/10.1016/j.rinp.2021.104695

[28] Shah, S. H., Arif, M., Qureshi, M. T., Safeen, A., Zaman, S., Ahmad, I., . . . , & Riaz, J. (2024). Investigation of structure, optoelectronic, and thermodynamic properties of gallium-based perovskites $GaMF_3$ (M = Ca, and Cd) for solar cell applications. *Optical and Quantum Electronics*, *56*(9), 1461. https://doi.org/10.1007/s11082-024-07354-y

[29] Ullah, S., Abbas, M., Tariq, S., Batoo, K. M., Rahman, N., Gul, U., . . . , & Ghani, M. U. (2024). Density functional quantum computations to investigate the physical prospects of lead-free chloro-perovskites $QAgCl_3$ (Q = K, Rb) for optoelectronic applications. *Transactions on Electrical and Electronic Materials*, *25*(3), 327–339. https://doi.org/10.1007/s42341-024-00514-7

[30] Javed, M. A., Ahmed, R., Tahir, S. A., & Ul Haq, B. (2025). Investigations of optoelectronic and scintillating properties of novel halide perovskites Cs_2KSnX_6 (X = Cl, Br, I). *Journal of Solid-State Chemistry*, *341*, 125084. https://doi.org/10.1016/j.jssc.2024.125084

[31] Li, C., Wang, A., Xie, L., Deng, X., Liao, K., Yang, J., . . . , & Hao, F. (2019). Emerging alkali metal ion (Li^+, Na^+, K^+ and Rb^+) doped perovskite films for efficient solar cells: Recent advances and prospects. *Journal of Materials Chemistry A*, *7*(42), 24150–24163. https://doi.org/10.1039/C9TA08130E

[32] Tabassum, M., Zia, Q., Zhou, Y., Reece, M. J., & Su, L. (2021). A review on advances in doping with alkali metals in halide perovskite materials. *SN Applied Sciences*, *3*(12), 888. https://doi.org/10.1007/s42452-021-04877-x

[33] Shimada, H., Oku, T., Ono, I., Suzuki, A., Iwakuni, H., Yamamoto, T., & Harada, K. (2025). Effects of light irradiation on the photovoltaic performance and crystal lattices of organic–inorganic perovskites in solar cells. *Next Energy*, *8*, 100263. https://doi.org/10.1016/j.nxener.2025.100263

[34] Pang, B., Cui, W., Li, Y., Feng, J., Dong, H., Yu, L., & Dong, L. (2025). Lithium and sodium ion Co-doping: A promising strategy for enhancing the performance of $Cs_2AgBiBr_6$ perovskite solar cells. *Journal of Alloys and Compounds*, *1010*, 177394. https://doi.org/10.1016/j.jallcom.2024.177394

[35] Mustafa, G. M., Akhtar, M. S., Sabir, U., Almaymoni, N. K., El-Fattah, W. A., Mnif, W., & Iqbal, M. (2026). Mechanistic insights into performance limitation and optimization of lead-free double perovskite Cs_2BiAgI_6 solar cells. *Journal of Sol-Gel Science and Technology*, *117*(2), 45. https://doi.org/10.1007/s10971-025-07102-y

[36] Su, D., Liu, G., Wei, R., Ma, M., Mu, Y., Yang, Z., & Zhang, G. (2024). Photovoltaic properties of alkali metal X (X = Li, Na, K, Rb, Cs) doped defective molybdenum diselenide structures: First principles study. *Solid State Communications*, *385*, 115502. https://doi.org/10.1016/j.ssc.2024.115502

[37] Awad, M. A., Shaban, M., & Rabia, M. (2022). The efficiency of M (M = Li, Na, or Cs) doped CdS nanomaterials in optoelectronic applications. *International Journal of Energy Research*, *46*(6), 8443–8451. https://doi.org/10.1002/er.7640

[38] Farooq, M. S., Alshahrani, D. O., Kanwal, S., Farooq, M. U., Ain, Q. U., & Saad, M. (2025). Enhanced structural and optoelectronics performance of perovskite solar cells via $MnSe_2$ incorporation in a $MAPbI_3$ absorber layer. *RSC Advances*, *15*(19), 14893–14902. https://doi.org/10.1039/d5ra02254a

[39] Zheng, D., Zhu, T., Yan, Y., & Pauporté, T. (2022). Controlling the formation process of methylammonium-free halide perovskite films for a homogeneous incorporation of alkali metal cations beneficial to solar cell performance. *Advanced Energy Materials*, *12*(13), 2103618. https://doi.org/10.1002/aenm.202103618

[40] He, L., Cao, P., Zhou, Z.-N., Yang, Y.-W., Chen, L.-Q., & Ye, Q. (2025). Alkali metal substitution for modulating three-dimensional halide double perovskite ferroelectric. *Inorganic Chemistry*, *64*(16), 8455–8462. https://doi.org/10.1021/acs.inorgchem.5c01211

[41] Fatima, S. K., Alzard, R. H., Amna, R., Alzard, M. H., Zheng, K., & Abdellah, M. (2025). Lead-free perovskites for next-generation applications: A comprehensive computational and data-driven review. *Materials Advances*, *6*(21), 7634–7661. https://doi.org/10.1039/d5ma00681c

[42] Zhou, X., Li, Z., Xu, O., Yuan, S., Huang, T., & Zou, B. (2026). Ultra-high-efficiency and reversible hydrochromism in a $CsCaCl_3$:Cd^{2+}/Mn^{2+} perovskite for advanced information encryption. *ACS Applied Materials & Interfaces*, *18*(1), 2009–2018. https://doi.org/10.1021/acsami.5c19903

[43] Tyagi, M., Zhuravleva, M., & Melcher, C. L. (2013). Theoretical and experimental characterization of promising new scintillators: Eu^{2+} doped $CsCaCl_3$ and $CsCaI_3$. *Journal of Applied Physics*, *113*(20), 203504. https://doi.org/10.1063/1.4807401

[44] Bourret-Courchesne, E. D., Bizarri, G. A., Borade, R., Gundiah, G., Samulon, E. C., Yan, Z., & Derenzo, S. E. (2012). Crystal growth and characterization of alkali-earth halide scintillators. *Journal of Crystal Growth*, *352*(1), 78–83. https://doi.org/10.1016/j.jcrysgro.2012.01.014

[45] Schwerdtfeger, P., Smits, O. R., & Pyykkö, P. (2020). The periodic table and the physics that drives it. *Nature Reviews Chemistry*, *4*(7), 359–380. https://doi.org/10.1038/s41570-020-0195-y

[46] Pyykkö, P. (2025). Is relativistic quantum chemistry a good theory of everything? *Pure and Applied Chemistry*, *97*(9), 1109–1114. https://doi.org/10.1515/pac-2025-0460

[47] Aktas, E., Rajamanickam, N., Pascual, J., Hu, S., Aldamasy, M. H., di Girolamo, D., . . . , & Abate, A. (2022). Challenges and strategies toward long-term stability of lead-free tin-based perovskite solar cells. *Communications Materials*, *3*(1), 104. https://doi.org/10.1038/s43246-022-00327-2

[48] Pingak, R. K., Ngara, Z. S., Johannes, A. Z., Bukit, M., Tanesib, J. L., Nitti, F., . . . , & Pasangka, B. (2024). DFT insights into the structural, mechanical, electronic and optical properties of novel $InZnCl_3$ and $InCdCl_3$ chloro-perovskites. *Indonesian Journal of Chemistry*, *24*(5), 1412–1428. https://doi.org/10.22146/ijc.94870

[49] Zhao, D., Choi, Y., Yokota, T., Someya, T., & Park, N. (2026). Halide perovskite radiation detectors: Conventional imaging applications and new opportunities. *Advanced Functional Materials*, *36*(6), e13676. https://doi.org/10.1002/adfm.202513676

[50] Blaha, P., Schwarz, K., Madsen, G. K. H., Kvasnicka, D., Luitz, J., Laskowski, R., . . . , & Marks, L. D. (2024). *WIEN2k: An augmented plane wave plus local orbitals program for calculating crystal properties*. Austria: Vienna University of Technology.

[51] Kassa, M., Debelo, N., & Woldemariam, M. (2023). The first-principles investigation of structural stability, mechanical, vibrational, thermodynamic, and optical properties of $CaHfS_3$ for optoelectronic application. *Advances in Condensed Matter Physics*, *2023*(1), 9332399. https://doi.org/10.1155/2023/9332399

[52] Saad, he., M, M., Khairy, A. M., Shirgawi, M. Y., Abdelrahman, A. H., Elhag, A., & Alsobhi, B. O. (2024). Crystal structure and optoelectronic properties of Rb-based metal halide perovskites $RbSiI_3$ and $RbGeI_3$: GGA–PBE study. *Bulletin of Materials Science*, *47*(3), 139. https://doi.org/10.1007/s12034-024-03209-0

[53] Srivastava, A. P., & Pandey, B. K. (2025). Analysis of the structural and electronic properties of TiO_2 under pressure using density functional theory and equation of state. *Computational Condensed Matter*, *44*, e01076. https://doi.org/10.1016/j.cocom.2025.e01076

[54] Jamal, M., Bilal, M., Ahmad, I., & Jalali-Asadabadi, S. (2018). IRelast package. *Journal of Alloys and Compounds*, *735*, 569–579. https://doi.org/10.1016/j.jallcom.2017.10.139

[55] Koller, D., Tran, F., & Blaha, P. (2011). Merits and limits of the modified Becke-Johnson exchange potential. *Physical Review B*, *83*(19), 195134. https://doi.org/10.1103/PhysRevB.83.195134

[56] Zhang, S., Chen, S., Chen, Y., Hou, J., Zhang, J., Liu, J., & Shi, Z. (2025). A DFT approach to explore the structural, mechanical, and optoelectronic of indium-based $InXY_3$ (X = Ca, Sr, Ba; Y = Cl, Br) halide perovskites for photoelectric applications. *Physics Letters A*, *533*, 130243. https://doi.org/10.1016/j.physleta.2025.130243

[57] Ullah, A., Sfina, N., Alshahrani, M. D., Alshehri, S., Tirth, V., Algahtani, A., . . . , & Ahmad, R. (2025). DFT analysis of wide band gap $TlBaCl_3$ and $CsBaCl_3$ chloroperovskites for UV applications. *Scientific Reports*, *15*(1), 33376. https://doi.org/10.1038/s41598-025-18037-3

[58] Thang, T. T., Linh, N. H., & Hung, D. T. (2025). Superior transport in SiSb and GeSb monolayers: Promising 2D candidates for advanced logic devices. *Vacuum*, *243*, 114821. https://doi.org/10.1016/j.vacuum.2025.114821

[59] Linh, N. H., Quang, T. T., Son, N. M., van Thanh, V., & Truong, D. V. (2023). Prediction of mechanical, electronic and optical properties of monolayer 1T Si-dichalcogenides via first-principles theory. *Materials Today Communications*, *36*, 106553. https://doi.org/10.1016/j.mtcomm.2023.106553

[60] Sun, S., Wang, C., Alghamdi, S., Zhou, H., Hao, Y., & Zhang, J. (2025). Recent advanced ultra-wide bandgap β-Ga_2O_3 material and device technologies. *Advanced Electronic Materials*, *11*(1), 2300844. https://doi.org/10.1002/aelm.202300844

[61] Rahman, M. A., Islam, S. S., Rayhan, M. A., Kabir, A., Alim, M. A., Uddin, J., . . . , & Hossain, M. K. (2024). Comparative analysis of KXH_3(X = Mg, Be) hydride cubic perovskites for hydrogen storage properties: A computational approach. *International Journal of Hydrogen Energy*, *80*, 725–732. https://doi.org/10.1016/j.ijhydene.2024.07.064

[62] Erum, N., & Ahmad, J. (2024). Structural, elastic and mechanical properties of cubic perovskite materials. *Archives of Advanced Engineering Science*, *2*(1), 24–29. https://doi.org/10.47852/bonviewAAES3202944

[63] Hill, R. (1952). The elastic behaviour of a crystalline aggregate. *Proceedings of the Physical Society. Section A*, *65*(5), 349–354. https://doi.org/10.1088/0370-1298/65/5/307

[64] Saeed, M., Haq, I. U., Rehman, S. U., Ali, A., Shah, W. A., Ali, Z., . . . , & Khan, I. (2021). Optoelectronic and elastic properties of metal halides double perovskites Cs_2InBiX_6. *Chinese Optics Letters*, *19*(3), 030004. https://doi.org/10.3788/COL202119.030004

[65] Tran, T. Q., Nguyen, H. L., Dinh, T. H., Toan, T. T., Do, V. T., Minh, S. N., & Trung, K. N. (2025). Modulation on electro-optical properties of p-PdS_2 monolayer by mechanical strain. In *Proceedings of the International Conference on Engineering Research and Applications*, *2*, 390–397. https://doi.org/10.1007/978-3-032-03859-3_42

[66] Wang, K., Zhang, X., & Wang, F. (2024). Exploring the electronic, mechanical, anisotropic and optical properties of the Sc-Al-C MAX phases from a first principles calculations. *Chemical Physics Letters*, *836*, 141024. https://doi.org/ https://doi.org/10.1016/j.cplett.2023.141024

[67] Thang, T. T., Linh, N. H., Hung, D. T., & van Truong, D. (2026). The AuS monolayer: Mechanical anisotropy, strain-tunable optoelectronic properties and high thermoelectric efficiency. *Computational and Theoretical Chemistry*, *1256*, 115617. https://doi.org/10.1016/j.comptc.2025.115617

[68] Khan, U. A., Khan, N. U., Abdullah, Alghtani., H, A., Tirth, V., Ahmed, S. J., . . . , & Zaman, A. (2022). First-principles investigation on the structural, electronic, mechanical and optical properties of silver based perovskite $AgXCl_3$ (X = Ca, Sr). *Journal of Materials Research and Technology*, *20*, 3296–3305. https://doi.org/10.1016/j.jmrt.2022.08.101

[69] Gao, Q., Ni, X., Liu, R., Luo, H., Zhou, J., Su, Y., . . . , & Liao, W.-H. (2026). Auxetic structures for energy absorption: A review on design, manufacturing, optimization, and applications. *Journal of Intelligent Material Systems and Structures*, *37*(5), 263–301. https://doi.org/10.1177/1045389X251381598

[70] Kim, D., Bae, Y., Kim, S., Choi, Y., Kim, H., Lim, S., . . . , & Park, T. (2026). Stretchable perovskite optoelectronics: Overcoming limitations via material and geometric approaches. *Advanced Energy Materials. Advance online publication*. https://doi.org/10.1002/aenm.202505956

[71] Bouhmaidi, S., Marjaoui, A., Talbi, A., Zanouni, M., Nouneh, K., & Setti, L. (2022). A DFT study of electronic, optical and thermoelectric properties of Ge-halide perovskites $CsGeX_3$ (X = F, Cl and Br). *Computational Condensed Matter*, *31*, e00663. https://doi.org/10.1016/j.cocom.2022.e00663

[72] Apon, I. A., Hasan, Md., R, M., & Islam, M. (2025). First-principles investigation of structural, mechanical, and electronic properties of $AMgX_3$ (A = Ga, In, Tl, and X = Cl, Br, I) perovskites for optoelectronic applications. *Physica Scripta*, *100*(1), 015931. https://doi.org/10.1088/1402-4896/ad966f

[73] Pan, Y., & Yang, F. (2024). Structural, hydrogen storage capacity, electronic and optical properties of Li-N-H hydrogen storage materials from first-principles investigation. *Journal of Energy Storage*, *87*, 111492. https://doi.org/10.1016/j.est.2024.111492

[74] Parajuli, D., Ramanjaneyulu, K., Murali, N., Ramakrishna, A., Batoo, K. M., Samatha, K., & Veeraiah, V. (2023). Structural, electronic, and optical properties of cubic perovskites $BiMO_3$ (M = Al, Ga & In) – A computational study. *Inorganic Chemistry Communications*, *158*, 111466. https://doi.org/10.1016/j.inoche.2023.111466

[75] Yuan, S., Ullah, M., & Tighezza, A. M. (2025). Impact of pressure on perovskite $MSnX_3$ (M = Li, Na; X = Cl, Br, I): A density functional theory study. *Frontiers in Energy*, *19*(3), 334–347. https://doi.org/10.1007/s11708-024-0970-4

[76] Hussain, M. K., Paudel, R., Kahdum, Jawad., B, & Syrotyuk, S. (2024). Optoelectronic and structural properties of bulk cubic perovskite $RbTaO_3$ and surface (0 0 1) for optoelectronic and spintronics applications. *Materials Chemistry and Physics*, *327*, 129778. https://doi.org/10.1016/j.matchemphys.2024.129778

[77] Li, B., Yao, Y., Kan, C., Hang, P., Xie, J., Yin, Q., . . . , & Yang, D. (2025). Promising excitonic absorption for efficient perovskite solar cells. *Joule*, *9*(2), 101780. https://doi.org/10.1016/j.joule.2024.10.012

[78] Hung, D. T., Linh, N. H., Quang, T. T., & van Truong, D. (2025). First-principles study on the mechanical properties and strain- and electric field-tunable electronic and optoelectronic behavior of MoA_2 (A = Se, Te) monolayers. *Surface Science*, *762*, 122831. https://doi.org/10.1016/j.susc.2025.122831

[79] Polyanskiy, M. N. (2024). Refractiveindex.info database of optical constants. *Scientific Data*, *11*(1), 94. https://doi.org/10.1038/s41597-023-02898-2

[80] Zhao, Y., Zhu, J., Wang, H., Ma, Z., Gao, L., Liu, Y., . . . , & He, J. (2021). Enhanced optical reflectivity and electrical properties in perovskite functional ceramics by inhibiting oxygen vacancy formation. *Ceramics International*, *47*(4), 5549–5558. https://doi.org/10.1016/j.ceramint.2020.10.139

[81] Chen, C., Zheng, S., & Song, H. (2021). Photon management to reduce energy loss in perovskite solar cells. *Chemical Society Reviews*, *50*(12), 7250–7329. https://doi.org/10.1039/D0CS01488E

How to Cite: Khan, S. A., Rahman, N., Ullah, S. Z., Sajjad, M., & Rehman, J. (2026). First-Principle Calculations of Structural, Electronic, Elastic, and Optical Properties of $XBaCl_3$ (X = In, Tl) Chloro-Perovskites. *Journal of Optics and Photonics Research*. https://doi.org/10.47852/bonviewJOPR62029251